Oxide Ion and Proton Conductivity in Highly Oxygen-Deficient Cubic Perovskite $SrSc_{0.3}Zn_{0.2}Ga_{0.5}O_{2.4}$

Chloe A. Fuller[a], Quentin Berrod[b,c], Bernhard Frick[c], Mark R. Johnson[c], Maxim Avdeev[d], John S. O. Evans[a]* and Ivana Radosavljevic Evans[a]*

[a]Department of Chemistry, Durham University, Science Site, South Road, Durham DH1 3LE, U.K.

[b]Université Grenoble Alpes, CNRS, CEA, IRIG-SyMMES, 38000 Grenoble, France

[c]Institut Laue Langevin, 71 Rue de Martyrs, 38000 Grenoble, France

[d]Australian Nuclear Science and Technology Organisation, Lucas Heights NSW 2234, Australia

SUPPLEMENTARY INFORMATION

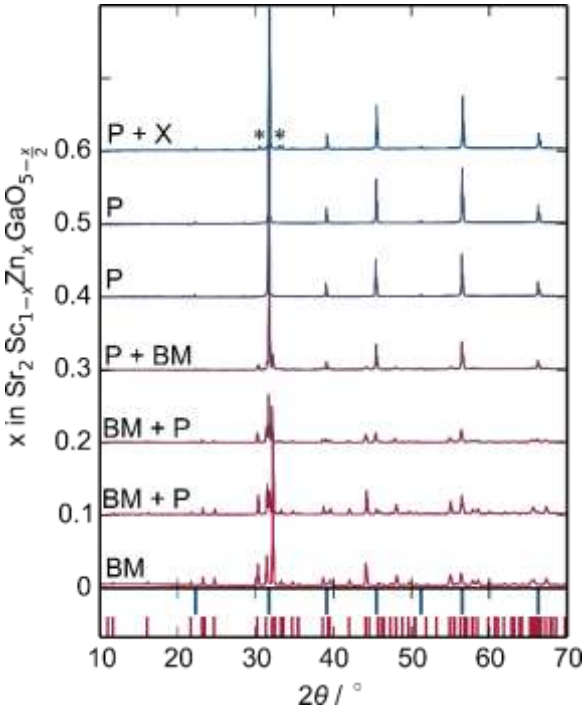

Figure S1. PXRD patterns of $Sr_2Sc_{1-x}Zn_xGaO_{5-x/2}$ with increasing *x*. Tick marks in the lower panel indicate the peak positions of the brownmillerite- (BM) and perovskite-type (P) phases in red and blue respectively. Asterisks mark the peaks produced by the unidentified impurity (X).

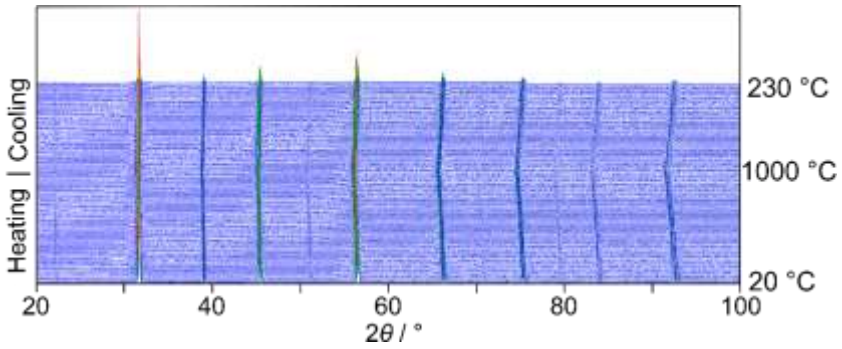

Figure S2. Plot showing the evolution of the X-ray diffraction pattern of SSZ40GO with temperature.

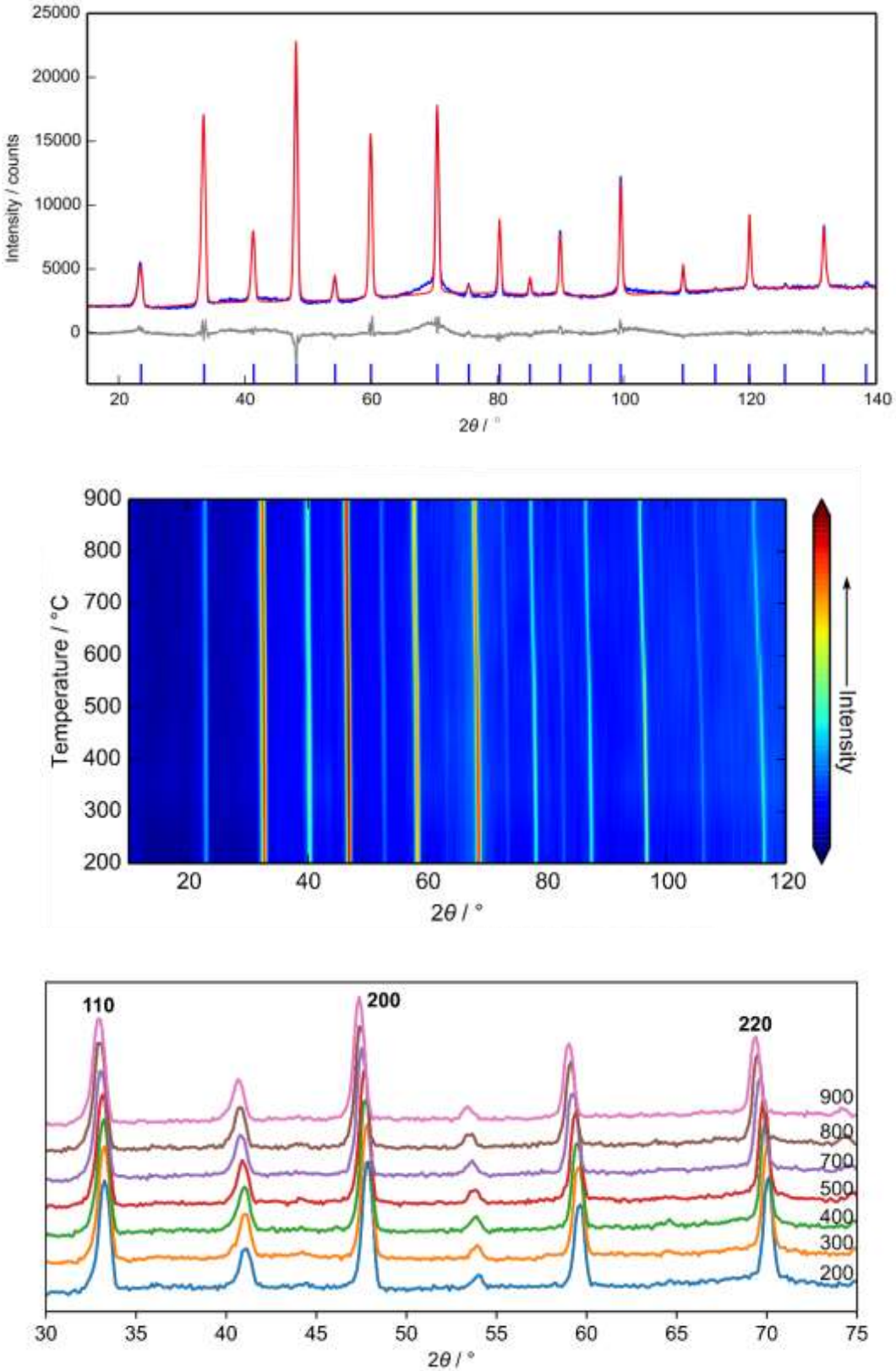

Figure S3. Top panel shows the neutron diffraction pattern of SSZ40GO at 20 K. Blue, red and grey lines show observed, calculated and difference curves respectively and the tick marks show the expected peak positions for the model. Middle panel shows a colour map of the variable temperature neutron diffraction patterns measured on ECHIDNA; bottom panel shows these data in the conventional way, zoomed onto the strongest peaks in the pattern.

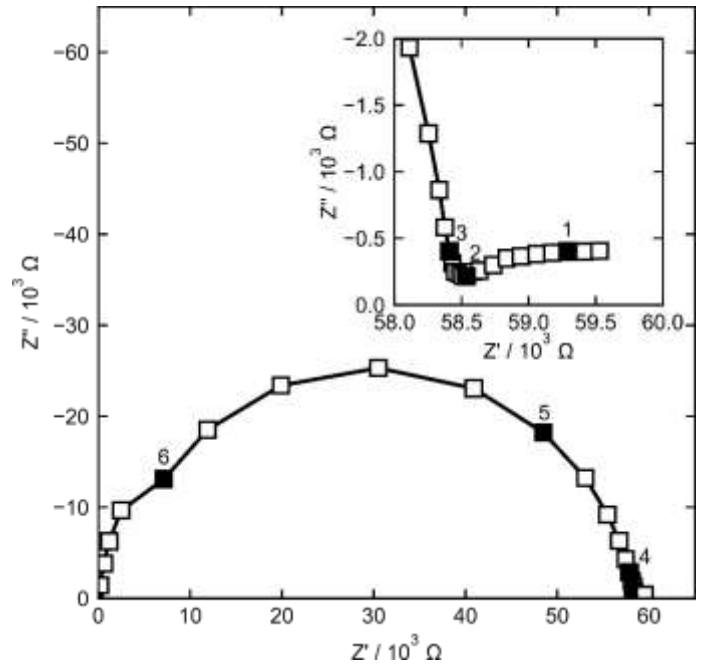

Figure S4. Complex impedance plot of SSZ40GO at 457 °C. Filled squares mark the specific frequencies where the number shows the frequency logarithm. The inset shows a zoom of the low frequency region. The dip at 10^6 Hz is a known instrument artefact.

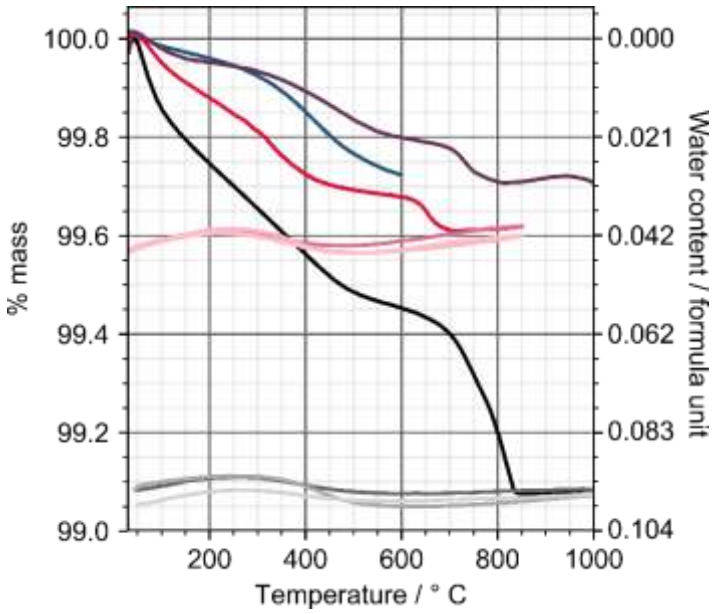

Figure S5. Multiple TGA traces from different experiments on SSZ40GO. Different heating rates and different samples of SSZ40GO were used. Samples take up differing amounts of water based on thermal history.

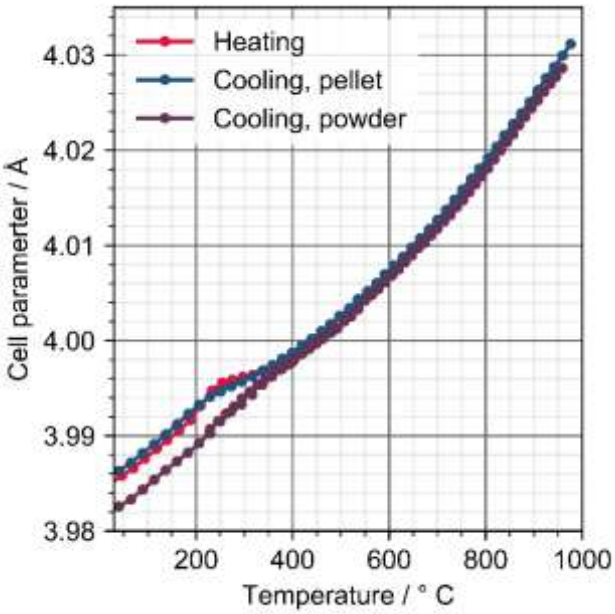

Figure S6. Unit cell parameters of SSZ40GO comparing the behaviour of pelleted and powdered samples. The heating data was measured on a pellet, but the same behaviour is observed in powders. On cooling, pelleted samples take up water on cooling whereas powdered samples do not.

Q-dependence of the QENS signal. The very low intensity of the QENS signal at low Q values does not allow us to determine the nature of the dynamic process observed (localised jumps vs confined diffusion). The left figure shows the data fitted with an elastic line and two Lorentzian functions: a broad one (4 meV half width at half maximum, HWHM, constant with Q, red dash line) and a narrow one (purple line). The intensity of the narrow component increases with Q, indicating a localized motion. Equivalent fits to the data can be obtained which show HWHM to be constant in Q (consistent with localized jumps, orange line in the right-hand figure) or to increase with Q (consistent with confined diffusion, blue line).

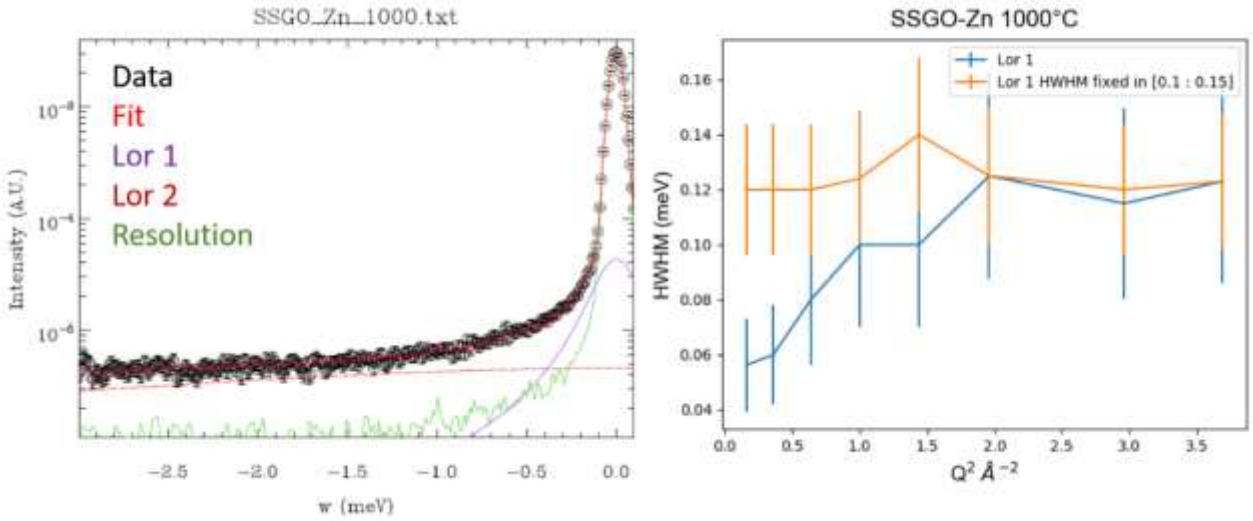

Figure S7. IN6-SHARP data fitted with an elastic line and two Lorentzian functions (Q = 1.92 $Å^{-1}$). The HWHM of the narrower component (Lor 1) is shown on the right. Two scenarios can be found (both showing an intensity increasing with Q): the HWHM is constant with Q (orange) or increases with Q (blue).

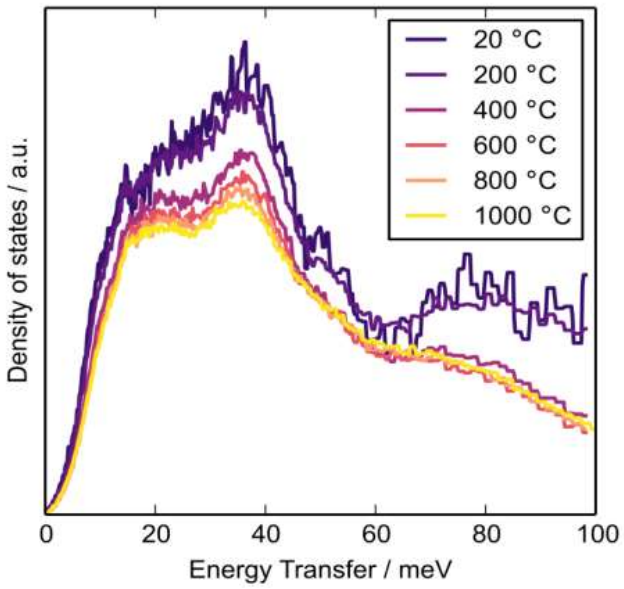

Figure S8. The phonon density of states extracted from data collected on the IN6 spectrometer.

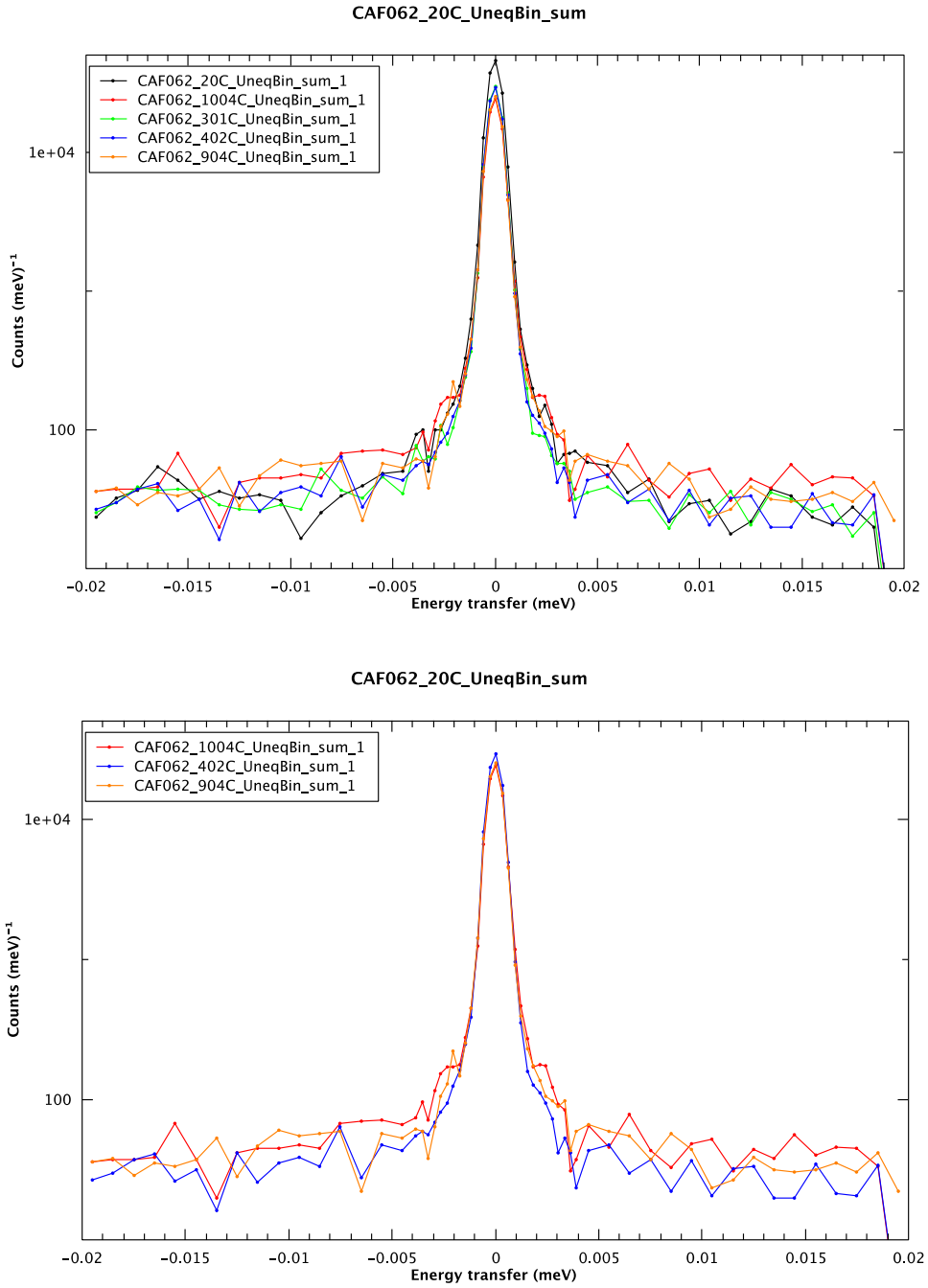

Figure S9. Inelastic spectra measured on IN16B in an energy range of ± 20μeV, summed over all detectors, energy binned and normalised to the elastic peak. Top shows spectra measured at all temperatures, bottom compares only the 400 °C spectrum with spectra measured at temperatures where the oxygen dynamics is expected based on the IFWS.

Solid state NMR. ^{45}Sc and ^{71}Ga solid state NMR experiments were performed to compare the local environments of these cations in SSGO and SSZ40GO. Spectra are shown in Figure S10. SSGO spectra are consistent with those previously reported and discussed in detail by Corallini et al. (J. Phys. Chem. C 2015, 119, 11447). Both the Sc and Ga bandwidths were much narrower for SSZ40GO, with a smaller quadrupolar coupling. This is consistent with a higher symmetry local environment compared to SSGO. For the Sc spectrum, the asymmetric shape suggests a spread of coupling constants resulting from a range of local environments. The Ga spectrum has a complex shape that suggests the presence of multiple Ga environments.

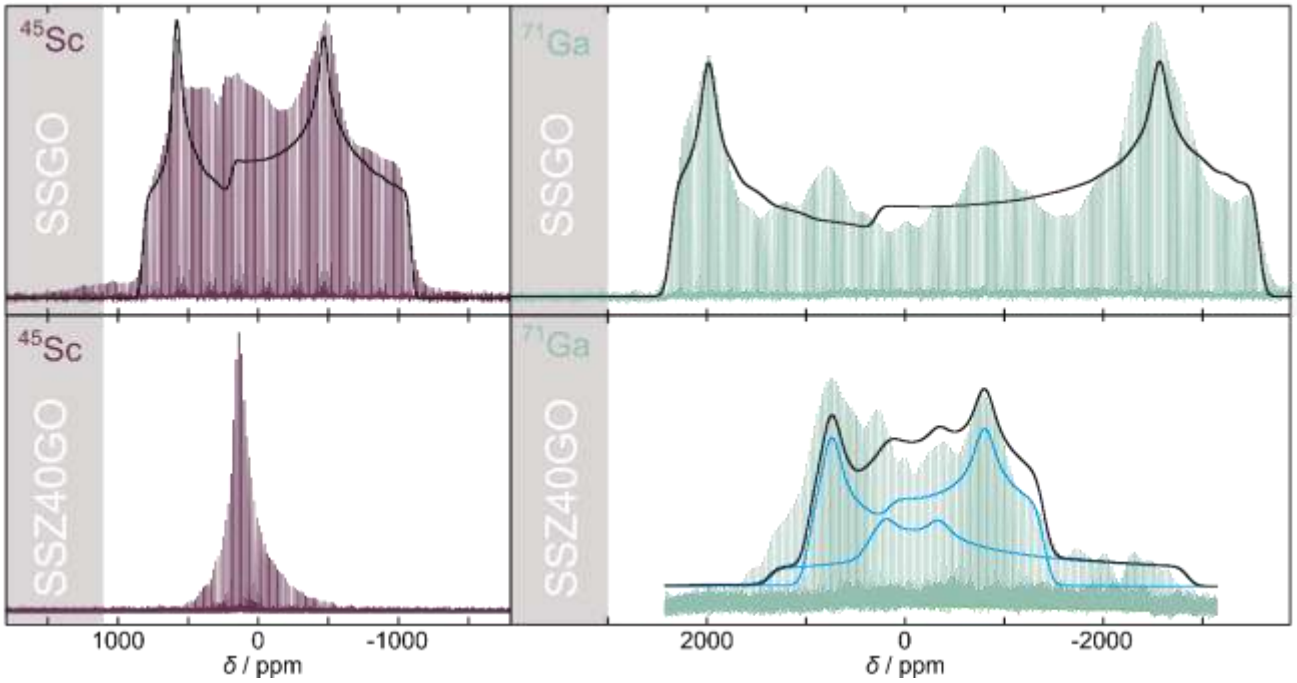

Figure S10. Solid state NMR spectra of SSGO (top) and SSZ40GO (bottom).

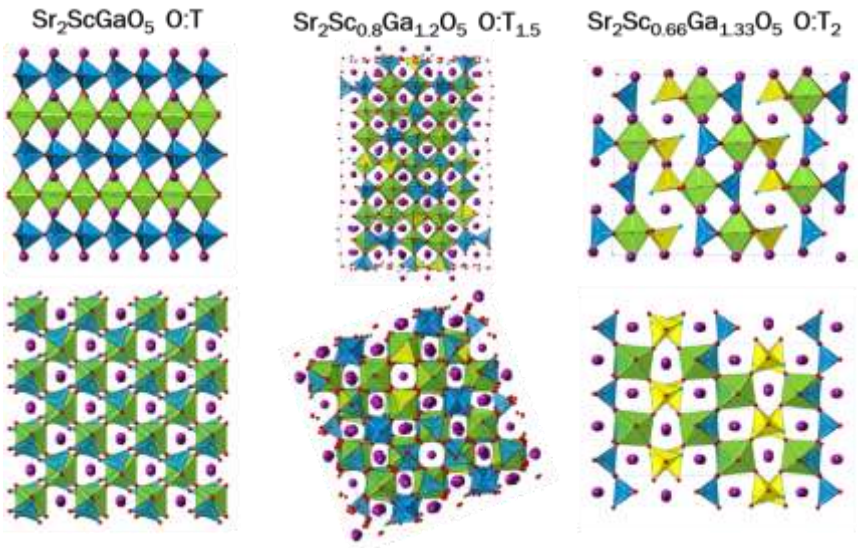

Figure S11. Structures of brownmillerite-type SSGO[5], $Sr_{10}Sc_6Ga_8O_{25}$[6] and $Ba_3ErGa_2O_{7.5}$[56] viewed along different axes showing the connectivity of the polyhedra as the Oh:T ratio is decreased. Purple and red spheres represent the A-site cation and oxygen respectively; green, blue and yellow polyhedra show $MO_{6/2}$ octahedra, $MO_{4/2}$ tetrahedra and $MO_{3/2}O$ units respectively.

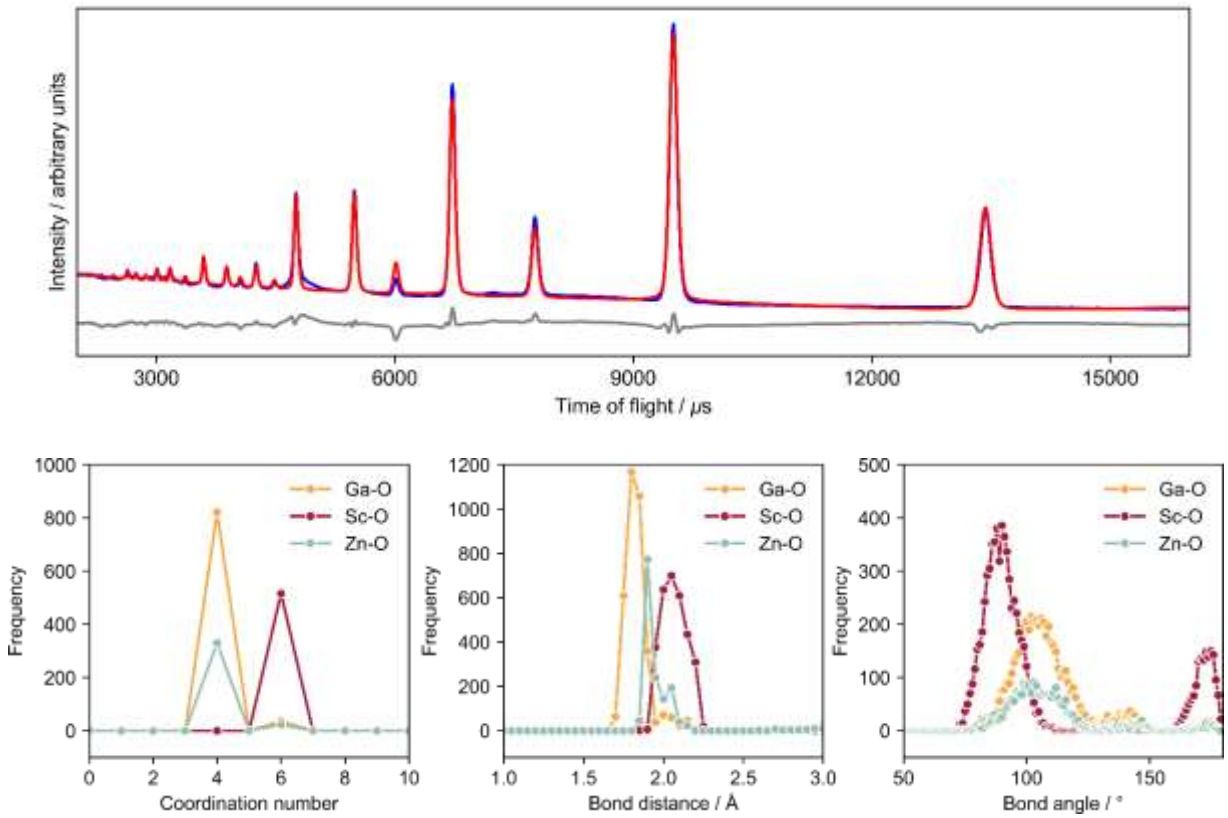

Figure S12. The top panel shows the fit to the Bragg data by the final OT2 model with red, blue and grey lines corresponding to the calculated, measured and difference patterns respectively. The bottom panel shows the distributions of coordination number, bond length and bond angle in the refined OT2 model

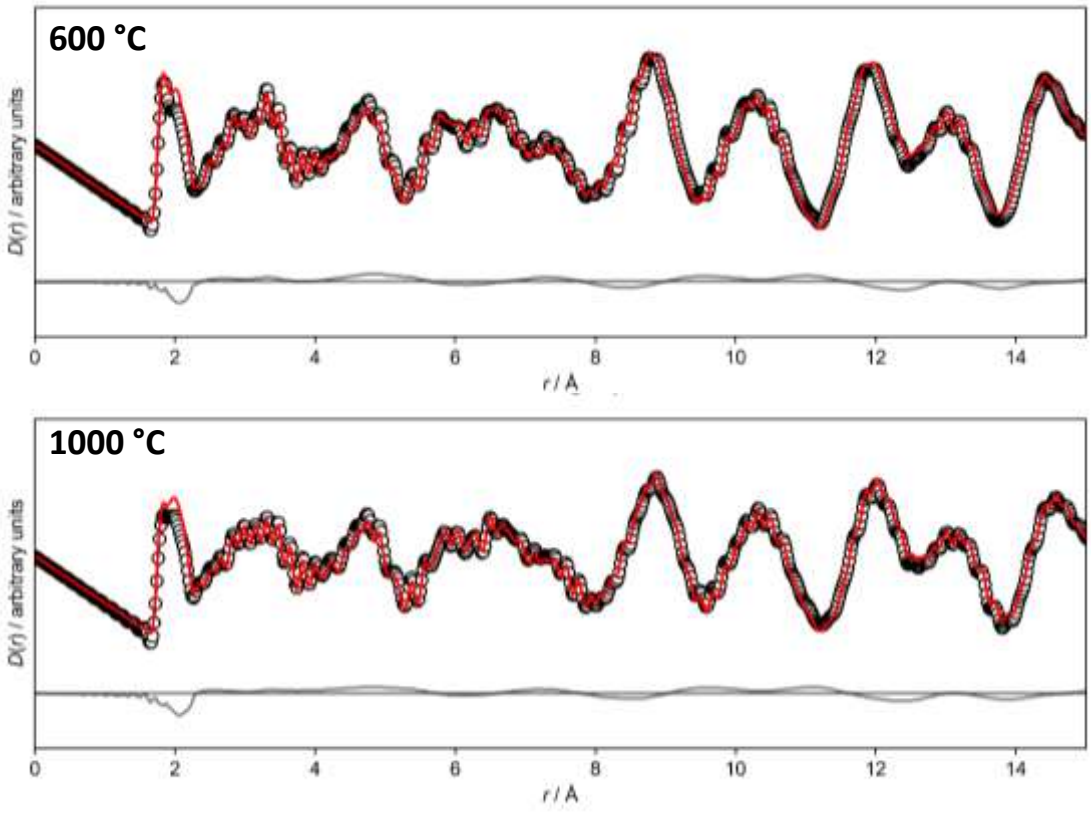

Figure S13. PDF fits of the final OT2 model at high temperatures.